Biomedical Optics EXPRESS

Fluorescence depletion properties of insulin–gold nanoclusters

Po-Fu Chen,[1] Chien-Liang Liu,[2] Wei-Kuan Lin,[1] Kuan-Chieh Chen,[1] Pi-Tai Chou,[2] and Shi-Wei Chu[1,3,*]

[1]*Department of Physics, National Taiwan University, No. 1, Sec. 4, Roosevelt Road, Taipei 10617, Taiwan*
[2]*Department of Chemistry, National Taiwan University, No. 1, Sec. 4, Roosevelt Road, Taipei 10617, Taiwan*
[3]*NTU Molecular Imaging Center, No. 81, Changxing St., Taipei 10672, Taiwan*
[*]*swchu@phys.ntu.edu.tw*

Abstract: Insulin–gold nanoclusters exhibit outstanding biocompatibility, photostability, and fluorescence quantum efficiency. However, they have never been used in superresolution microscopy, which requires nonlinear switching or saturation of fluorescence. Here we examine the fluorescence and stimulated emission depletion properties of gold nanoclusters. Their bleaching rate is very slow, demonstrating superior photostability. Surprisingly, however, the best depletion efficiency is less than 70%, whereas the depletion intensity requirement is much higher than the expectation from a simple two-level model. Fluorescence lifetime measurement revealed two distinct lifetime components, which indicate intersystem and reverse intersystem crossing during excitation. Based on population dynamic calculation, excellent agreement of the maximal depletion efficiency is found. Our work not only features the first examination of STED with metallic clusters, but also reveals the significance of molecular transition dynamics when considering a STED labeling.

OCIS codes: (180.1790) Confocal microscopy; (160.2540) Fluorescent and luminescent materials; (250.6715) Switching; (160.4236) Nanomaterials; (160.1435) Biomaterials

References and links

1. E. Betzig, G. H. Patterson, R. Sougrat, O. W. Lindwasser, S. Olenych, J. S. Bonifacino, M. W. Davidson, J. Lippincott-Schwartz, and H. F. Hess, "Imaging intracellular fluorescent proteins at nanometer resolution," Science **313**(5793), 1642–1645 (2006).
2. B. Huang, W. Wang, M. Bates, and X. Zhuang, "Three-dimensional super-resolution imaging by stochastic optical reconstruction microscopy," Science **319**(5864), 810–813 (2008).
3. S. W. Hell, "Far-field optical nanoscopy," Science **316**(5828), 1153–1158 (2007).
4. M. Yamanaka, Y. Yonemaru, S. Kawano, K. Uegaki, N. I. Smith, S. Kawata, and K. Fujita, "Saturated excitation microscopy for sub-diffraction-limited imaging of cell clusters," J. Biomed. Opt. **18**(12), 126002 (2013).
5. S. W. Chu, T. Y. Su, R. Oketani, Y. T. Huang, H. Y. Wu, Y. Yonemaru, M. Yamanaka, H. Lee, G. Y. Zhuo, M. Y. Lee, S. Kawata, and K. Fujita, "Measurement of a saturated emission of optical radiation from gold nanoparticles: application to an ultrahigh resolution microscope," Phys. Rev. Lett. **112**(1), 017402 (2014).
6. R. Heintzmann, T. M. Jovin, and C. Cremer, "Saturated patterned excitation microscopy--a concept for optical resolution improvement," J. Opt. Soc. Am. A **19**(8), 1599–1609 (2002).
7. V. Westphal, S. O. Rizzoli, M. A. Lauterbach, D. Kamin, R. Jahn, and S. W. Hell, "Video-rate far-field optical nanoscopy dissects synaptic vesicle movement," Science **320**(5873), 246–249 (2008).
8. D. Wildanger, R. Medda, L. Kastrup, and S. W. Hell, "A compact STED microscope providing 3D nanoscale resolution," J. Microsc. **236**(1), 35–43 (2009).
9. E. Rittweger, K. Y. Han, S. E. Irvine, C. Eggeling, and S. W. Hell, "STED microscopy reveals crystal colour centres with nanometric resolution," Nat. Photonics **3**(3), 144–147 (2009).
10. T. Grotjohann, I. Testa, M. Leutenegger, H. Bock, N. T. Urban, F. Lavoie-Cardinal, K. I. Willig, C. Eggeling, S. Jakobs, and S. W. Hell, "Diffraction-unlimited all-optical imaging and writing with a photochromic GFP," Nature **478**(7368), 204–208 (2011).

#241016 Received 15 Jun 2015; revised 23 Jul 2015; accepted 23 Jul 2015; published 28 Jul 2015

11. C. A. J. Lin, C. H. Lee, J. T. Hsieh, H. H. Wang, J. K. Li, J. L. Shen, W. H. Chan, H. I. Yeh, and W. H. Chang, "Synthesis of fluorescent metallic nanoclusters toward biomedical application: recent progress and present challenges," J. Med. Biol. Eng. **29**, 276–283 (2009).
12. X. M. Wen, P. Yu, Y. R. Toh, A. C. Hsu, Y. C. Lee, and J. Tang, "Fluorescence dynamics in BSA-protected Au-25 nanoclusters," J. Phys. Chem. C **116**(35), 19032–19038 (2012).
13. C. L. Liu, H. T. Wu, Y. H. Hsiao, C. W. Lai, C. W. Shih, Y. K. Peng, K. C. Tang, H. W. Chang, Y. C. Chien, J. K. Hsiao, J. T. Cheng, and P. T. Chou, "Insulin-directed synthesis of fluorescent gold nanoclusters: preservation of insulin bioactivity and versatility in cell imaging," Angew. Chem. Int. Ed. Engl. **50**(31), 7056–7060 (2011).
14. B. Harke, J. Keller, C. K. Ullal, V. Westphal, A. Schönle, and S. W. Hell, "Resolution scaling in STED microscopy," Opt. Express **16**(6), 4154–4162 (2008).
15. S. W. Hell, "Toward fluorescence nanoscopy," Nat. Biotechnol. **21**(11), 1347–1355 (2003).
16. E. K. Yeow, S. M. Melnikov, T. D. Bell, F. C. De Schryver, and J. Hofkens, "Characterizing the fluorescence intermittency and photobleaching kinetics of dye molecules immobilized on a glass surface," J. Phys. Chem. A **110**(5), 1726–1734 (2006).
17. J. Hotta, E. Fron, P. Dedecker, K. P. F. Janssen, C. Li, K. Müllen, B. Harke, J. Bückers, S. W. Hell, and J. Hofkens, "Spectroscopic rationale for efficient stimulated-emission depletion microscopy fluorophores," J. Am. Chem. Soc. **132**(14), 5021–5023 (2010).
18. S. H. Yau, O. Varnavski, J. D. Gilbertson, B. Chandler, G. Ramakrishna, and T. Goodson III, "Ultrafast optical study of small gold monolayer protected clusters: a closer look at emission," J. Phys. Chem. C **114**(38), 15979–15985 (2010).
19. B. Huang, M. Bates, and X. Zhuang, "Super-resolution fluorescence microscopy," Annu. Rev. Biochem. **78**(1), 993–1016 (2009).
20. J. Zheng, P. R. Nicovich, and R. M. Dickson, "Highly fluorescent noble-metal quantum dots," Annu. Rev. Phys. Chem. **58**(1), 409–431 (2007).

1. Introduction

Superresolution optical microscopies have been actively developed during the last decade to resolve cellular features down to tens of nanometers. Representative examples that rely on switching fluorescence on–off include photoactivated localization microscopy (PALM) [1], stochastic optical reconstruction microscopy (STORM) [2], and stimulated emission depletion (STED) microscopy [3]. Another category that relies on saturation of signals includes saturated excitation (SAX) microscopy [4, 5] and saturated structured-illumination microscopy (SSIM) [6].

Compared to SSIM, PALM, and STORM, STED microscopy does not require repetitive image acquisition to allow subsequent image reconstruction and therefore provides a faster imaging rate (28 frames/s with 62-nm lateral resolution in living cells) [7]. Furthermore, STED can be easily combined with a confocal laser scanning system to provide unprecedented three-dimensional nano-imaging capability with much better resolution than SAX microscopy [8]. Therefore, in this work, we focus on STED microscopy.

One of the major challenges in STED microscopy is to find appropriate dyes, since STED requires an extraordinarily strong depletion beam. The ideal label for STED should exhibit not only outstanding photostability, but also bright emission to compensate for fluorescence loss due to depletion [9, 10]. Both requirements can be met by protein-protected metallic nanoclusters, such as bovine-serum-albumin-protected Au_{25} nanoclusters and insulin–gold nanoclusters (IGNCs) [11–13]. An IGNC is essentially fluorescent insulin with a 1-nm Au core at its center. The physiological function of insulin is preserved during synthesis; thus, IGNCs are expected to give insights into insulin-related diseases such as diabetes, Alzheimer's disease, obesity, and aging [13]. In comparison with nitrogen vacancies in diamond, which are arguably the most stable fluorescence emitters [9], IGNCs possess the advantages of low toxicity and high biocompatibility, and do not disturb the biological functions of the labeled bioentities.

The resolution of STED microscopy is $R_{STED} \approx R_{confocal} \Big/ \sqrt{1 + I_{dep} / I_s}$ [3, 14]. R_{STED} and R_{confocal} denote the resolution in STED and confocal microscopies, respectively. I_{dep} is the intensity of the depletion light, and I_{s} is the saturation intensity of a fluorescent molecule. The saturation intensity is defined as the depletion light intensity at which the fluorescence becomes half of the initial value. From this equation, the resolution of STED microscopy is

#241016 Received 15 Jun 2015; revised 23 Jul 2015; accepted 23 Jul 2015; published 28 Jul 2015

better with higher I_{dep} or lower I_s. However, a strong depletion intensity would potentially damage fragile biological specimens, so the better strategy is to reduce I_s.

Using a simple two-level transition model, the saturation intensity can be defined as $I_s = hc/\lambda \cdot \sigma \cdot \tau$, where h is Planck's constant, c is the speed of light in vacuum, λ is the excitation wavelength, and σ and τ denote the absorption cross section and fluorescence lifetime of the fluorophore, respectively [3, 15]. The reported fluorescence lifetime of IGNCs is 2 μs, which is much longer than that of common fluorescent markers [13]. From Mie theory estimation, when the excitation wavelength is 490 nm, the absorption cross section is ~4×10^{-16} cm^2, and the corresponding saturation intensity should be 5×10^2 W/cm^2, which is much lower than that of most reported labels [3, 15]. In combination with its biocompatibility and stable fluorescent characteristics, these properties make IGNCs an attractive choice as fluorescent markers for STED microscopy. However, there is no report of STED on fluorescent nanoclusters yet. In this paper, we examine the STED properties of IGNCs and study their photostability with and without the STED beam. We will show that the simple two-level model estimation is insufficient, and a more sophisticated molecular transition model will be necessary to account for the STED property of IGNCs.

2. Experimental setup

Our experimental scheme is shown in Fig. 1. It is a confocal microscope (IX71 and FV300, Olympus, Japan) equipped with a supercontinuum laser source (SC400-PP-HE, Fianium, UK), which provides both the excitation and depletion sources through a home-built wavelength selector. The laser repetition rate is 2 MHz, and the pulsewidth is 110 ps. The absorption of IGNCs lies mainly in the ultraviolet to blue spectral range, and their emission peaks around 640 nm, as shown in Fig. 1(a). Since the supercontinuum source is relatively weak in the violet regime, we choose two bands at 480–500 nm and 690–720 nm as the excitation and depletion sources, respectively. The powers of the excitation and depletion beams are 100 μW and 4 mW, respectively, at the focal point. In the experiment, an apochromatic objective (UPlanSApo 60XW, NA = 1.2, Olympus, Japan) was used, and the resultant spatial overlap of the excitation and depletion beams in the axial direction of the focal region is shown in Fig. 1(b), where a 0.2-μm deviation is found. During image acquisition, a suitable dichroic mirror (FF505/606-Di01, Semrock, NY, USA) and barrier filters (FF01-629/53, Semrock, NY, USA & BA565IF, Olympus, Japan) are inserted in the confocal system. The pixel dwell time is 6 μs. Fluorescence signals are typically acquired by averaging a 10×10 μm^2 area.

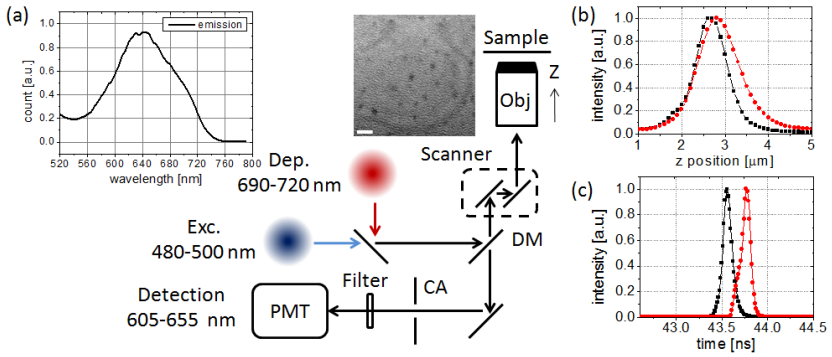

Fig. 1. (a) Schematics of the experimental setup. The excitation and depletion beams are combined and sent into a laser scanning confocal microscope. The epi-collected fluorescence is guided through a dichroic mirror (DM), confocal aperture (CA), and suitable filters before reaching the photomultiplier tube (PMT). Insets show the emission spectrum and TEM image of IGNCs (scale bar: 5 nm). (b) Axial overlap and (c) temporal separation of the excitation (black) and depletion (red) beams.

#241016 Received 15 Jun 2015; revised 23 Jul 2015; accepted 23 Jul 2015; published 28 Jul 2015

For fluorescence lifetime measurement, a time-correlated single-photon counting system (SPC-150, Becker & Hickl, Germany) plus a spectral detector (Polychromator MS 125 & PML-16-1-C, Becker & Hickl, Germany) is adopted. The same setup can also be used to determine the temporal separation of the excitation and depletion pulses. To efficiently deplete the fluorescence, the excitation pulse reached the sample first, followed by the depletion pulse after a ~200 ps delay, as shown in Fig. 1(c).

The preparation of IGNCs follows our previous publication [13]. Briefly, by mixing insulin and $HAuCl_4$ in a Na_3PO_4 buffer and continuously stirring at 4 °C for 12 h, fluorescent IGNCs were synthesized. The crude product was centrifuged (4000*g*) for 30 min with a cutoff of 5 kDa to obtain purified IGNCs. In this experiment, the IGNCs are fixed on a slide glass by the dried droplet method and protected with a cover glass. A transmission electron microscopy (TEM) image of the IGNCs is shown in the inset of Fig. 1(a).

3. Results

Figure 2(a) demonstrates the fluorescence depletion of an IGNC film. The inset shows fluorescent images of an IGNC film before and after depletion, illustrating loss of fluorescence. The black dots show the intensity dependence of the depletion process, where the vertical axis represents the spontaneous fluorescence intensity (I_{fluo}) divided by the initial fluorescence intensity (I_0). The red curve shows the exponential fitting of the depletion, and the corresponding equation is given in the figure. As expected, the depletion ratio is larger when the depletion beam intensity increases. However, there are two surprising observations. The first is that the maximal depletion ratio reaches only 60%, although the depletion intensity has reached a few gigawatts per centimeter squared. From the exponential fitting, at least 30% background is still present even if a higher intensity is applied. The second one is the saturation intensity (I_s), which can be found when the fluorescence drops to 50% and is unexpectedly as high as 2.8 GW/cm^2.

Figure 2(b) shows the bleaching of the IGNC fluorescence with and without the depletion beam. When there is only an excitation beam at an intensity of 0.07 GW/cm^2 (the red curve and red triangles), the fluorescence of the IGNCs is extraordinarily stable. Quantitatively, it takes more than 500 s to bleach half of the initial fluorescence. On the other hand, when the depletion beam overlaps the excitation beam, the bleaching becomes slightly faster (the green curve and black rectangles). The intensity of the depletion beam is 3.6 GW/cm^2, which is adequate to suppress more than half of the initial fluorescence. To demonstrate the reversibility of fluorescence depletion, the depletion beam is turned on and off repeatedly. As expected, when the depletion beam is on, the fluorescence drops appreciably; when the depletion beam is off, the fluorescence intensity returns. Nevertheless, it is clear that the fluorescence does not return to its initial value because of bleaching. Quantitatively, 30% bleaching was found after 120-s illumination with excitation and depletion beams.

#241016 Received 15 Jun 2015; revised 23 Jul 2015; accepted 23 Jul 2015; published 28 Jul 2015

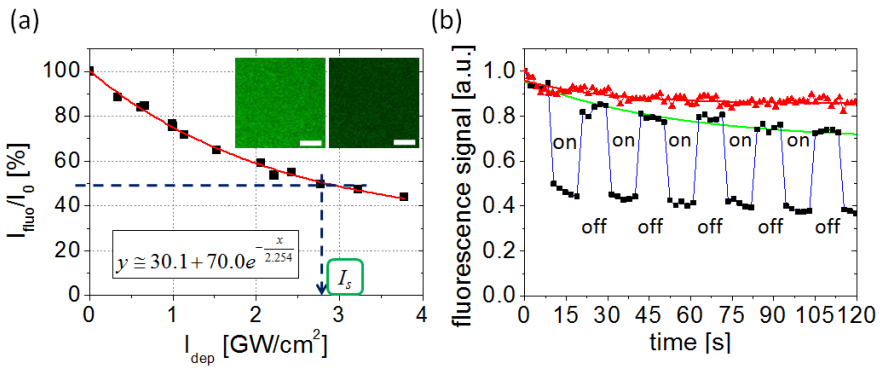

Fig. 2. (a) Fluorescence depletion curve of an IGNC film. Black rectangles are experimental results, and the corresponding exponential fitting is given as an equation and a red curve. Inset shows initial fluorescence image (exc. only) and image after depletion (exc. + dep.). Scale bar: 2 μm. Blue dashed line marks the position of 50% depletion and the corresponding value of I_s. (b) Bleaching of IGNC fluorescence and its reversible depletion. Red triangles and curve show photobleaching with only an excitation beam on IGNC film; green curve shows photobleaching when the depletion beam is added. The fluorescence can be repetitively switched on and off, as shown by the black rectangles.

4. Discussion

We have demonstrated the STED capability of IGNCs for the first time and examined the depletion power dependency, saturation intensity, and photostability. From Fig. 2(b), slight photobleaching is observed with only the excitation beam, whereas slightly more bleaching appears when a repetitive depletion beam is added for on–off switching. Compared to other STED markers, such as Atto565 (excited in air), its fluorescence drops 30% after ~450 s of illumination at a light intensity of several watts per centimeter squared [16]. Considering that the excitation intensity is much higher in our experiment and that our pixel dwell time is not particularly short, the photostability of IGNCs is indeed outstanding.

In addition, the insignificant increase in bleaching when the depletion beam is added indicates that excited state absorption (ESA) is not dominant in fluorescence depletion [17]. The lifetime of transient absorption in gold nanoclusters is known to be only a few picoseconds [18], so it is reasonable that ESA does not play a major role when the depletion pulse is delayed by 200 ps after the pump pulse.

From Fig. 2(a), the STED saturation intensity of IGNCs is as high as a few gigawatts per centimeter squared, which is larger than the average requirement of typical STED fluorescent labeling [3, 15, 19] and is also much larger than our calculated value based on a simple two-level calculation (~500 W/cm^2). One possible reason is that the parameters we used in the two-level calculation, such as the fluorescence lifetime and cross section, are incorrect. The result of lifetime measurement is shown in Fig. 3(a). There are two lifetime components, 42.5 ns and 0.4 ns. Both are significantly shorter than the reported value in Ref [13]. However, even if we use the shorter lifetime component to calculate the saturation intensity, the result is 2.5×10^6 W/cm^2, which is still much lower than our measured value. Alternatively, the value that we used for the cross section might be incorrect. However, to fit the measured saturation intensity at 2.8 GW/cm^2, the cross section has to be as small as 10^{-18} cm^2. Although this is still a reasonable number, the simple two-level model cannot explain the existence of the undepleted background.

#241016 Received 15 Jun 2015; revised 23 Jul 2015; accepted 23 Jul 2015; published 28 Jul 2015

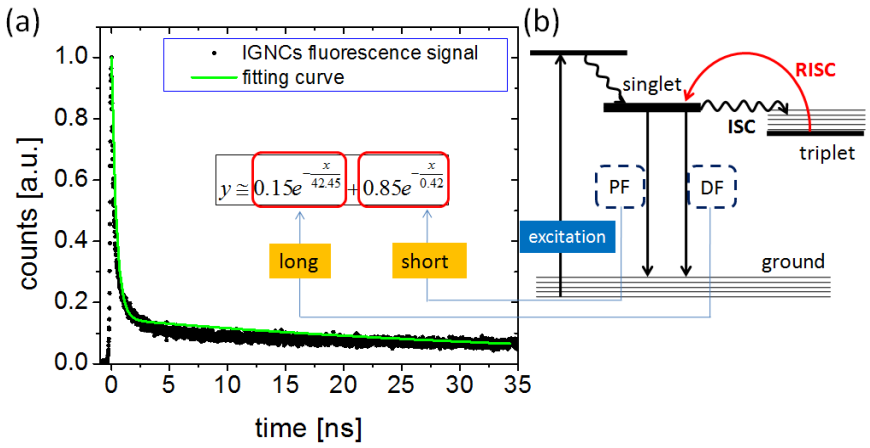

Fig. 3. (a) Fluorescence lifetime measurement of IGNC film. Green line is the fitting with two exponential components, whose corresponding lifetimes and coefficients are given in the inset equation. (b) Schematic of energy levels of IGNCs. The ISC and RISC processes are shown. PF: prompt fluorescence; DF: delayed fluorescence.

According to a previous study of protein-protected metallic nanoclusters, there is a triplet state in gold nanoclusters [12]. When a gold nanocluster is excited, the excited electrons exhibit a substantial probability of crossing into the triplet state, known as intersystem crossing (ISC). Those electrons trapped in the triplet state may return to the normal fluorescence state (singlet state) because of thermal activation, and the process is termed reverse intersystem crossing (RISC). A schematic of ISC and RISC is shown in Fig. 3(b). According to the model, there should be two fluorescence lifetime components. One is prompt fluorescence, which comes from direct transition between the singlet and ground states, i.e., spontaneous emission, exhibiting a short lifetime component. The other is delayed fluorescence due to the ISC and RISC mechanism, which generates a long lifetime component. This model corresponds well to our lifetime measurement in Fig. 3(a), where two fluorescence lifetime components are found. To explain the limitation of the depletion ratio, Eq. (1) gives the population distribution estimation based on the first-order transition dynamics.

$$\frac{d[S]_t}{dt} = -k_f[S]_t - k_{isc}[S]_t + k_{risc}[T]_t;\ \frac{d[T]_t}{dt} = k_{isc}[S]_t - k_{risc}[T]_t - k_p[T]_t, \quad (1)$$

where $[S]_t$ and $[T]_t$ denote the population in the singlet and triplet state at time t. At $t = 0$, corresponding to the arrival of the excitation pulse, $[S]$ is equal to $[S]_0$, and $[T]_0$ is zero. Further, k_f, k_p, k_{isc}, and k_{risc} denote the transition rate from the singlet to ground state, triplet to ground state, singlet to triplet state, and triplet to singlet state, respectively. Assuming k_f, k_p << k_{isc}, k_{risc}, we derived the population distribution at time t,

#241016 Received 15 Jun 2015; revised 23 Jul 2015; accepted 23 Jul 2015; published 28 Jul 2015

$$[S]_t = [S]_0 \left\{ \frac{k_{risc}}{k_{isc}+k_{risc}} e^{-\left(\frac{k_f + k_p \frac{k_{isc}}{k_{risc}}}{1+\frac{k_{isc}}{k_{risc}}}\right)t} + \frac{k_{isc}}{k_{isc}+k_{risc}} e^{-(k_{isc}+k_{risc})t} \right\};$$

$$[T]_t = [S]_0 \left\{ \frac{k_{isc}}{k_{isc}+k_{risc}} e^{-\left(\frac{k_f + k_p \frac{k_{isc}}{k_{risc}}}{1+\frac{k_{isc}}{k_{risc}}}\right)t} - \frac{k_{isc}}{k_{isc}+k_{risc}} e^{-(k_{isc}+k_{risc})t} \right\} . \quad (2)$$

Since the instantaneous fluorescence intensity is proportional to $k_f\,[S]_t$, by comparison with the lifetime measurement in Fig. 3(a), the rate constants in Eq. (2) can be quantitatively determined. As a result, at t = 0.2 ns, when the depletion pulse arrives, 2.5% of the initial population has been relaxed to the ground state through fluorescence. The remaining population ratio in the singlet state is 97.5% × ($[S]_{0.2}$/($[S]_{0.2}$ + $[T]_{0.2}$) = 66.35%, and that in the triplet state is 97.5% × $[T]_{0.2}$/($[S]_{0.2}$ + $[T]_{0.2}$) = 31.15%. Therefore, a substantial amount of the population is transferred to the triplet state when the depletion pulse arrives. Since the transition moment between the triplet and ground states is extremely small, the population in the triplet state cannot be depleted via the STED beam. Looking back to Fig. 2(a), at least 30% of the fluorescence cannot be depleted, corresponding very well to our population calculation.

We tried several approaches to enhance the depletion efficiency. A depletion beam with a shorter wavelength (610–630 nm) was adopted to reduce the chromatic aberration, but this laser band excites more fluorescence than depletion. IGNCs in aqueous solution were tested with STED, but to our surprise, no suppression was observed at all. Gated detection was also examined, and no significant improvement of the depletion ratio was found. One possible strategy is to reduce the delay between the excitation and the depletion pulse, so that more population can be depleted before going into the triplet state. However, in our current setup, the pulse width is about 100 ps, limited by the supercontinuum source. Therefore, it is difficult to reduce the delay significantly. If a shorter delay is necessary, a shorter pulse is required. Nevertheless, two more issues might appear when adopting a short pulse laser. One is that two-photon excitation may start to affect the fluorescence response, resulting in even more complicated transition dynamics. The other is that the wavelength requirement (480-500 nm for excitation, 690-720 nm for depletion) is not easily achievable with conventional femtosecond/picosecond laser sources. It may be accessible by a Ti:sapphire laser and a optical parametric oscillator system, with a subsequent frequency doubling setup, which will greatly increase not only complexity but also cost of the whole imaging system.

Another possible approach to enhance the maximum depletion efficiency is to inhibit the transition to the triplet state. Unfortunately, fast reversible intersystem crossing is an intrinsic property for the gold nanodots, similar to most of the molecules/clusters consisting of heavy atom such as Au. The heavy atom effect induces a large spin-orbit coupling matrix, which leads to substantial mixing between singlet and triplet states. This will also reduce the energy gap, $\Delta E_{S\text{-}T}$, between singlet and triplet states, resulting in the ($T_1 \rightarrow S_1$) reverse intersystem crossing and hence the thermally activated fluorescence delay. Nevertheless, it may be worthwhile to study the size dependent $\Delta E_{S\text{-}T}$ for the gold nanodots. By increasing the size of gold nanodots, it has been well established that the corresponding emission wavelength could be tuned from blue to near infrared [20]. Accordingly, $\Delta E_{S\text{-}T}$ may be changed as well. In the case of increasing $\Delta E_{S\text{-}T}$ for certain size (emission wavelength) of gold nanodots, the reduction of S_1-T_1 mixing will inhibit the intersystem crossing to the triplet state.

#241016 Received 15 Jun 2015; revised 23 Jul 2015; accepted 23 Jul 2015; published 28 Jul 2015

5. Conclusion

We observed the STED capability of IGNC fluorescence for the first time. Outstanding photostability of IGNCs was demonstrated, and a reversible STED process was confirmed. However, we found that the maximal depletion ratio is ~60%, with an unexpectedly high saturation intensity at a few gigawatts per centimeter squared. Fluorescence lifetime measurement of the IGNCs revealed two states with significantly different lifetimes, indicating ISC and RISC mechanisms during fluorescence emission. The delayed fluorescence due to ISC and RISC results in incomplete fluorescence depletion even with a very high depletion intensity. Although ultimately IGNCs might not be a good fluorescent marker for STED microscopy, our study opens up a new direction to consider when selecting suitable STED labels.

Acknowledgments

We gratefully acknowledge the financial support of the Ministry of Science and Technology (NSC-101-2923-M-002-001-MY3, NSC 102-2112-M-002-018-MY3) and the NTU Molecular Imaging Center.

#241016 Received 15 Jun 2015; revised 23 Jul 2015; accepted 23 Jul 2015; published 28 Jul 2015